Cell Reports
Medicine

Article

ASN007 is a selective ERK1/2 inhibitor with preferential activity against RAS-and RAF-mutant tumors

Graphical abstract

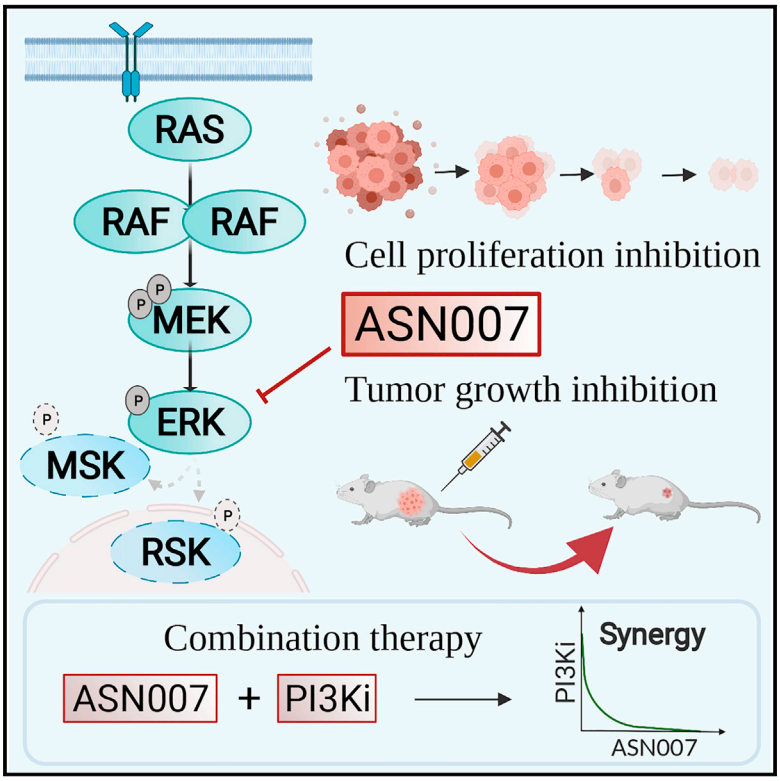

Authors

Ana Portelinha, Scott Thompson, Roger A. Smith, ..., Louis Denis, Anas Younes, Sanjeeva Reddy

Correspondence

scott.thompson@asanabio.com (S.T.), anas.younes@astrazeneca.com (A.Y.)

In brief

Portelinha et al. describe a selective ERK1/2 kinase inhibitor, ASN007, with antitumor activity against several solid tumors and lymphomas. Moreover, the authors show that PI3K inhibition enhances the activity of ASN007.

Highlights

- ASN007 is a reversible ATP-competitive inhibitor of ERK1 and ERK2 kinase activity
- The presence of RAS/RAF pathway mutations predicts enhanced efficacy of ASN007
- ASN007 demonstrates strong efficacy in a resistant melanoma PDX model
- Combination with a PI3K inhibitor enhances ASN007 antitumor activity in several tumors

Portelinha et al., 2021, Cell Reports Medicine 2, 100350
July 20, 2021
https://doi.org/10.1016/j.xcrm.2021.100350

CellPress

Cell Reports Medicine

CellPress
OPEN ACCESS

Article

ASN007 is a selective ERK1/2 inhibitor with preferential activity against RAS- and RAF-mutant tumors

Ana Portelinha,[1] Scott Thompson,[5,*] Roger A. Smith,[5] Mariana Da Silva Ferreira,[1] Zahra Asgari,[1] Andrea Knezevic,[2] Venkatraman Seshan,[2] Elisa de Stanchina,[3] Sandeep Gupta,[5] Louis Denis,[5] Anas Younes,[1,4,6,8,*] and Sanjeeva Reddy[5,7]

[1]Department of Medicine, Memorial Sloan Kettering Cancer Center, New York, NY, USA
[2]Department of Epidemiology and Biostatistics, Memorial Sloan Kettering Cancer Center, New York, NY, USA
[3]Antitumor Assessment Core, Memorial Sloan Kettering Cancer Center, New York, NY, USA
[4]Lymphoma Service, Memorial Sloan Kettering Cancer Center, New York, NY, USA
[5]Asana BioSciences, Lawrenceville, NJ, USA
[6]Present address: AstraZeneca, Medimmune Way, Gaithersburg, MD 20878, USA
[7]Present address: Oncology Business Unit, Bayer HealthCare, Whippany, NJ, USA
[8]Lead contact
*Correspondence: scott.thompson@asanabio.com (S.T.), anas.younes@astrazeneca.com (A.Y.)
https://doi.org/10.1016/j.xcrm.2021.100350

SUMMARY

Inhibition of the extracellular signal-regulated kinases ERK1 and ERK2 (ERK1/2) offers a promising therapeutic strategy in cancers harboring activated RAS/RAF/MEK/ERK signaling pathways. Here, we describe an orally bioavailable and selective ERK1/2 inhibitor, ASN007, currently in clinical development for the treatment of cancer. In preclinical studies, ASN007 shows strong antiproliferative activity in tumors harboring mutations in BRAF and RAS (KRAS, NRAS, and HRAS). ASN007 demonstrates activity in a $BRAF^{V600E}$ mutant melanoma tumor model that is resistant to BRAF and MEK inhibitors. The PI3K inhibitor copanlisib enhances the antiproliferative activity of ASN007 both *in vitro* and *in vivo* due to dual inhibition of RAS/MAPK and PI3K survival pathways. Our data provide a rationale for evaluating ASN007 in RAS/RAF-driven tumors as well as a mechanistic basis for combining ASN007 with PI3K inhibitors.

INTRODUCTION

The mitogen-activated protein kinase (MAPK) pathway, also known as the RAS-RAF-MEK-ERK pathway, regulates a variety of physiologic cell functions, including cell proliferation and survival.[1,2] RAS activation by upstream receptors requires a switch from the guanosine diphosphate (GDP)-bound to the guanosine triphosphate (GTP)-bound form. This conformational change leads to RAF binding, promoting its dimerization and activation.[3] Activated RAF phosphorylates and activates mitogen-activated protein/extracellular signal-regulated kinase (MEK) which phosphorylates and activates ERK1/2 at threonine and tyrosine sites. ERK regulates a variety of cell functions by phosphorylating >200 cytoplasmic and nuclear substrates.[4,5]

This physiologic pathway is frequently hijacked by cancer cells, through activating mutations in RAS and RAF genes.[1,2,6] From a therapeutic point of view, this activated pathway can be targeted at different node levels. To date, only drugs targeting BRAF (vemurafenib, dabrafenib, and encorafenib) or MEK (trametinib, binimetinib, and cobimetinib) have been approved by regulatory agencies for the treatment of $BRAF^{V600E}$ mutant melanoma.[4,7–13] Newer strategies are exploring targeting the most proximal node, RAS, or the most distal node, ERK1/2. Several ERK1/2 inhibitors are in development, including ulixertinib (BVD-523), ravoxertinib (GDC-0994), and SCH772984.[14–16] Rationale for these strategies is aimed at improving the quality and duration of clinical responses achieved by RAF and MEK inhibitors, to overcome acquired resistance, which may include activation of ERK1/2 through a feedback mechanism, and to broaden tumor types that may benefit from inhibiting this pathway.[4,14,17,18]

In this study, we describe a potent and selective ERK1/2 inhibitor, ASN007, which is in clinical development for the treatment of cancer. We show that ASN007 has broad antiproliferative activity in both solid tumors and lymphoma, with preferential sensitivity in RAS and BRAF mutant cancers. We also describe enhanced antitumor activity *in vitro* and *in vivo* using a combinational treatment of ASN007 and a phosphatidylinositol 3-kinase (PI3K) inhibitor.

RESULTS

Discovery and biochemical characterization of the selective ERK1/2 inhibitor ASN007

The imidazole carboxamide scaffold was used as a starting point to discover and develop potent and selective inhibitors

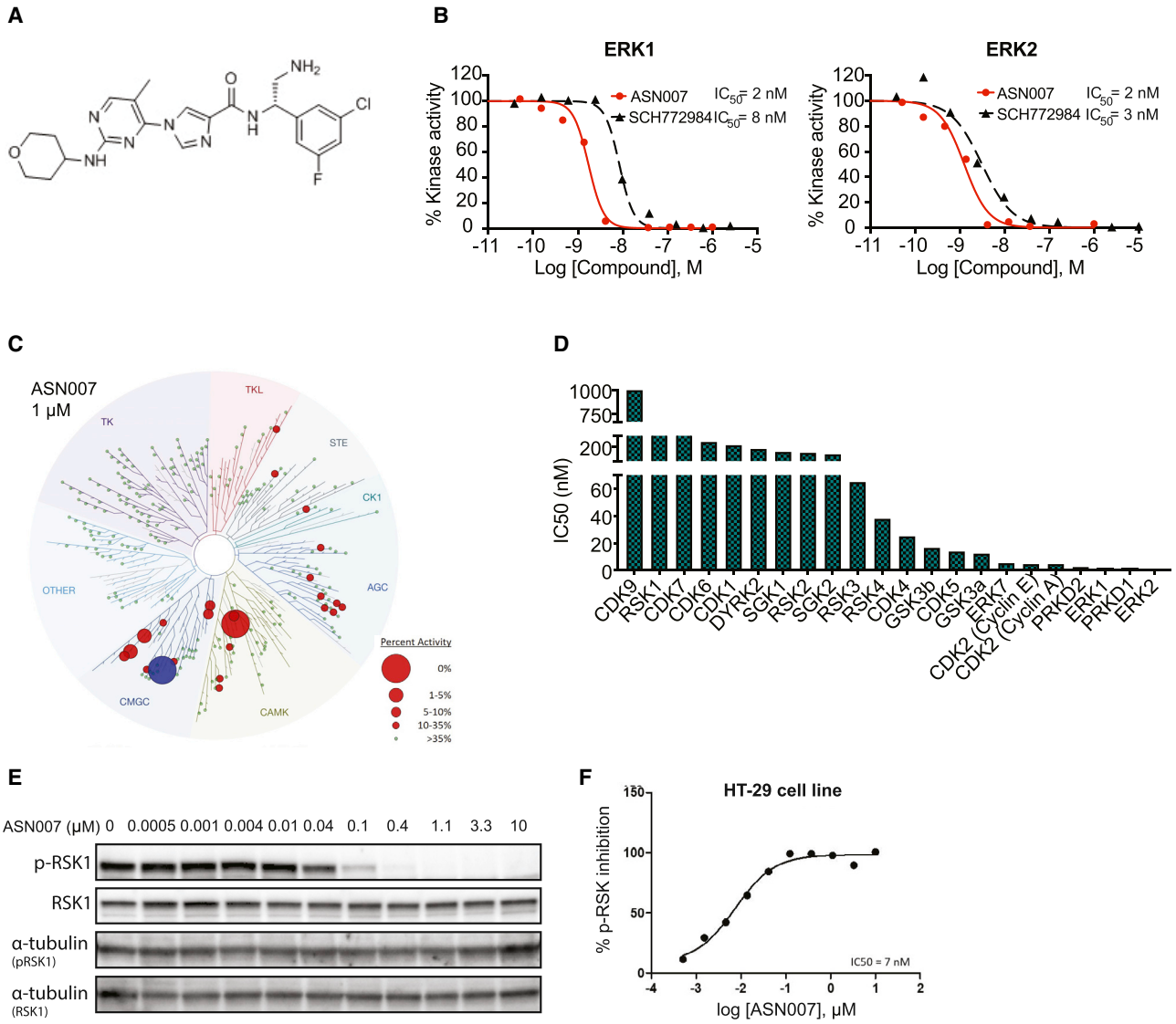

Figure 1. Structural and biochemical characterization of ASN007

(A) Molecular structure of ASN007, MW = 473.

(B) Dose-response curves of ERK1/2 inhibitors (ASN007 or SCH772894) in a homogeneous time-resolved fluorescence (HTRF)-based ERK1/2 enzymatic activity assay.

(C) Kinome tree dendrogram showing the biochemical kinase profiling assay (KinaseProfiler, Eurofiler), which measures the kinase inhibitory activity of ASN007 in a radiometric enzymatic assay in a panel of 335 purified kinases. Hit kinases reported are marked with a red circle and the size of the circle indicates the relative potency of ASN007 for each kinase. ERK1/2 kinases are illustrated by a blue circle. Green dots indicate kinases against which ASN007 does not have significant activity at 1 μM. The dendrogram was generated using the web tool TREESpot, provided by DiscoverX.

(D) IC_{50} values (nM) for ASN007 against the top 22 kinases, which showed >75% inhibition at 1 μμM, identified from the primary kinome screening.

(E) Dose-dependent effect of ASN007 treatment on phosphorylation of ERK1/2 targets. Representative western blot analysis shows inhibition of RSK1 (Ser380) phosphorylation after 4h of ASN007 treatment in a colorectal adenocarcinoma cell line, HT-29.

(F) Dose-response curve of ASN007 inhibition of RSK phosphorylation in the human colon cancer HT-29 $BRAF^{V600E}$ mutant cell line, measured by an ELISA test.

of ERK1 and ERK2 kinases. A structure-activity-based approach was used to systematically modify the key moieties of the compounds to optimize the pharmacological features, comprising synthesis and testing of >600 compounds. The evaluation of multiple parameters such as potency and selectivity for ERK kinase inhibition, cell-based mechanistic and anti-proliferative activity, pharmacokinetics, and *in vivo* efficacy led to the identification of ASN007, *N*-(2-amino-1-(3-chloro-5-fluorophenyl)ethyl)-1-(5-methyl-2-((tetrahydro-2*H*-pyran-4-yl) amino)pyrimidin-4-yl)-1*H*-imidazole-4-carboxamide (Figure 1A) as a promising lead compound for further development. In cell-free biochemical assays, ASN007 inhibited ERK1 and ERK2 with a half-maximal inhibitory concentration (IC_{50}) value of 2 nM against both kinases (Figure 1B). In comparison,

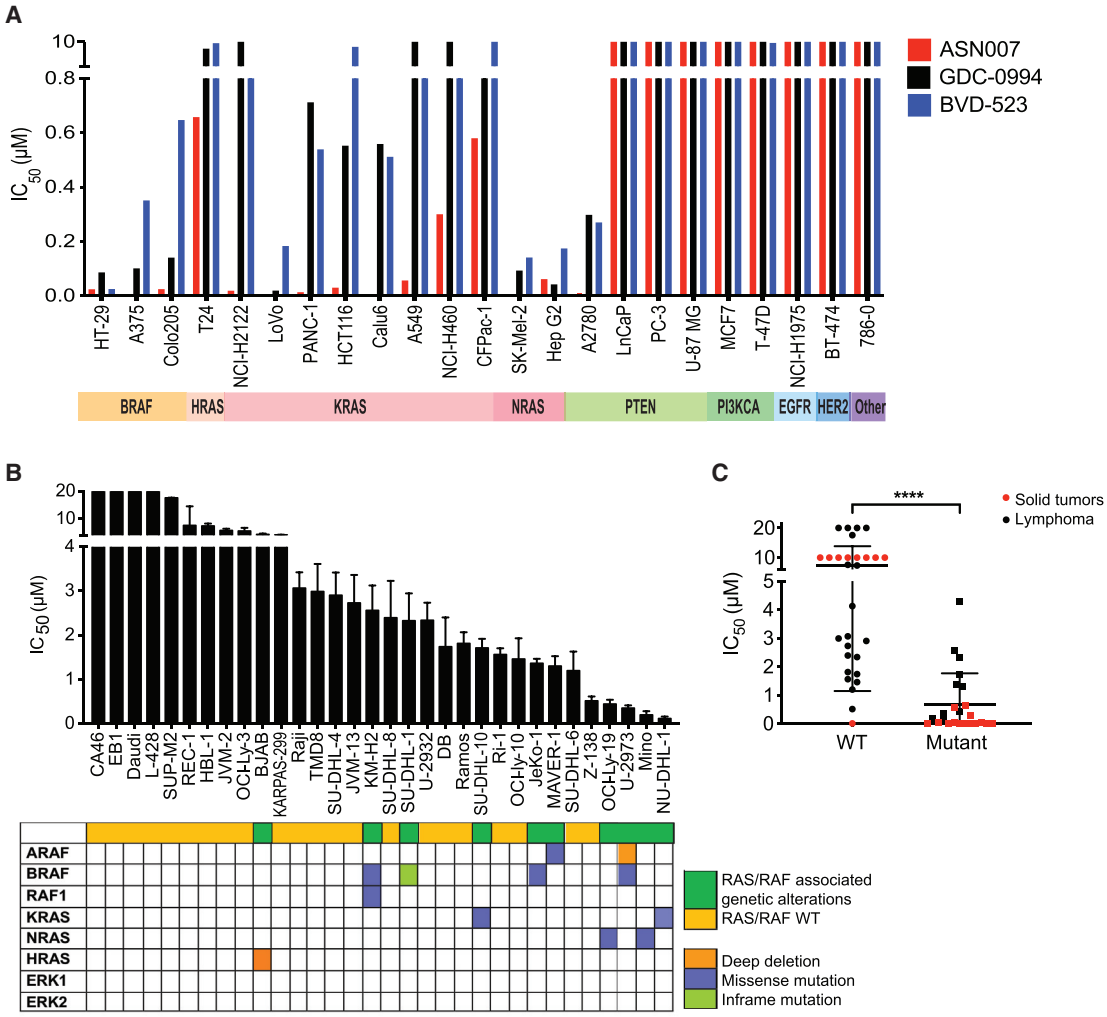

Figure 2. Antiproliferative efficacy of ASN007 in solid tumor and lymphoma cell lines

(A) The IC_{50} values of ASN007 were compared with two other ERK1/2 inhibitors (ulixertinib/BVD-523 and ravoxertinib/GDC-0994) in a panel of solid tumor cell lines with or without mutations in the RAS/RAF/MEK/ERK pathway. Cells were treated with increasing concentrations of the specified ERK1/2 inhibitor for 72 h before cell viability assessment.

(B) ASN007 was more effective against lymphoma cell lines harboring mutations in the RAS/RAF pathway. Each bar represents the mean ± SD of three independent experiments.

(C) Dot plot comparing IC_{50} values of ASN007 in cell lines with or without mutations in the RAS/RAF/MAPK pathway. Black dots illustrate IC_{50} values for lymphoma cell lines and red dots illustrate solid tumor cell lines. Differences between groups were calculated with Student's t test. ****$p < 0.0001$.

SCH772984 showed IC_{50} values of 8 and 3 nM against ERK1 and ERK2, respectively.

In a primary kinome screening assay comprising a panel of 335 serine/threonine, tyrosine, and protein lipid kinases, ASN007 demonstrated a selective inhibition of ERK1/2 kinases at 1.0 μM concentration (Figure 1C; Table S1). IC_{50} determination for the top 22 kinases, which showed >75% inhibition at 1 μM, confirmed the selectivity of ASN007 for ERK1 and ERK2, in addition to the inhibition of a small number of kinases belonging to the CMGC and CAMK kinase subfamilies (Figure 1D).

ASN007 treatment promotes the dose-dependent decrease in the phosphorylation level of ERK1/2 protein targets RSK-1 and FRA-1 in HT-29, a colorectal cancer cell line harboring $BRAF^{V600E}$ mutation (data not shown; Figure 1E). The inhibitory effect of ASN007 on RSK-1 phosphorylation was further confirmed in an enzyme-linked immunosorbent assay (ELISA) (Figure 1F). The inhibition of ERK1/2 targets MSK1 and RSK1 was observed as early as 15 min with ASN007 treatment and lasted for at least 72 h, as shown by time-dependent analysis in a mantle cell lymphoma (JeKo-1) and a melanoma (A375) cell line (Figure S1A). The antiproliferative activity of ASN007 was mainly due to the induction of a time-dependent cell-cycle arrest in the G0/G1 phase (Figure S1B; Table S2).

The potential functional effects of the inhibition of the off-target kinases were investigated in both *in vitro* cell lines and *in vivo* tumor xenograft models. ASN007 demonstrated no

Table 1. IC_{50} values for representative RAS and RAF mutant cell lines

Cell line	Tissue	Gene mutated	Mutation (RAS pathway)	IC_{50} (μM) ASN007	GDC-0994	BVD-523
HT-29	colon	BRAF	V600E	0.020	0.082	0.021
A375	skin	BRAF	V600E	0.007	0.097	0.347
Colo 205	colon	BRAF	V600E	0.021	0.137	0.643
T24	bladder	HRAS	G12V	0.653	8.335	9.512
NCI-H2122	lung	KRAS	G12C	0.015	>10	2.050
LoVo	colon	KRAS	G13D	0.005	0.015	0.179
PANC-1	pancreas	KRAS	G12D	0.009	0.708	0.535
HCT116	colon/rectum	KRAS	G13D	0.026	0.549	8.762
Calu-6	lung	KRAS	Q61K	0.007	0.555	0.508
A549	lung	KRAS	G12C	0.053	>10	2.350
NCI-H460	lung	KRAS	Q61H	0.296	>10	3.3000
CFPAC-1	pancreas	KRAS	G12V	0.576	3.601	>10
SK-MEL-2	skin	NRAS	Q61R	0.003	0.089	0.137
Hep G2	liver	NRAS	Q61L	0.058	0.038	0.170
A2780	ovary	PTEN	N/A	0.008	0.294	0.266
LNCaP	prostate	PTEN	N/A	>10	>10	>10
PC-3	prostate	PTEN	N/A	>10	>10	>10
U-87 MG	brain	PTEN	N/A	>10	>10	>10
MCF7	breast	PIK3CA	N/A	>10	>10	>10
T-47D	breast	PIK3CA	N/A	>10	>10	9.566
NCI-H1975	lung	EGFR	N/A	>10	>10	>10
BT-474	breast	HER2	N/A	>10	>10	>10
786-O	kidney	Other	N/A	>10	>10	>10

N/A, not applicable.

evidence of the mechanistic inhibition of CDK2, CDK4, GSK3, or PRDK1, confirming its selectivity in cells (Figure S1C) and tumors (Figure S1D).

Table 2. IC_{50} mean values (μM) of ASN007 against different lymphoma cell lines

Cell line	IC_{50}	Cell line	IC_{50}
CA46	>10	SU-DHL-8	2.4
EB1	>10	SU-DHL-1	2.3
Daudi	>10	U-2932	2.3
L-428	>10	DB	1.7
SUP-M2	>10	Ramos	1.8
REC-1	7.6	SU-DHL-10	1.7
HBL-1	7.4	Ri-1	1.6
JVM-2	5.7	OCI-Ly10	1.5
OCI-Ly3	5.5	JeKo-1	1.4
BJAB	4.3	MAVER-1	1.3
KARPAS-299	4.1	SU-DHL-6	1.2
Raji	3.1	Z-138	0.5
TMD8	3.0	OCI-Ly19	0.4
SU-DHL-4	2.9	U-2973	0.3
JVM-13	2.7	MINO	0.2
KM-H2	2.6	NU-DHL-1	0.1

Preferential activity of ASN007 against RAS/RAF pathway mutant cancers

The antiproliferative activity of ASN007 was assessed in a panel of 23 solid tumor cell lines with (n = 14) or without (n = 9) genetic alterations in the RAS/RAF pathway (Figure 2A). Similar to the ERK1/2 inhibitors GDC-0994 and BVD-523, ASN007 showed preferential antiproliferative activity in cell lines harboring mutations in the RAS/RAF pathway, with a median IC_{50} of 37 nM (range, 13–100 nM), compared to IC_{50} values of >10,000 nM in cell lines without the mutations (Table 1). However, ASN007 demonstrated greater potency compared to GDC-0994 and BVD-523 in cell lines harboring RAS/RAF mutations (Figure 2A). Similar results were observed in a panel of lymphoma cell lines (n = 32) representing a wide range of histologic subtypes (Figure 2B). The compound was particularly potent against $KRAS^{A146T}$ mutant cell line NU-DHL-1, $NRAS^{G13D}$ mutant cell line MINO, and $BRAF^{V600E}$ mutant lymphoma cell line U-2973, with IC_{50} values of 100, 200, and 300 nM, respectively (Table 2). Thus, the presence of RAS/RAF pathway mutations was predictive of the enhanced efficacy of ASN007, irrespective of the tumor type (Figure 2C).

In vivo activity of ASN007

ASN007 activity was also evaluated in four different human tumor xenograft mouse models harboring either KRAS or NRAS

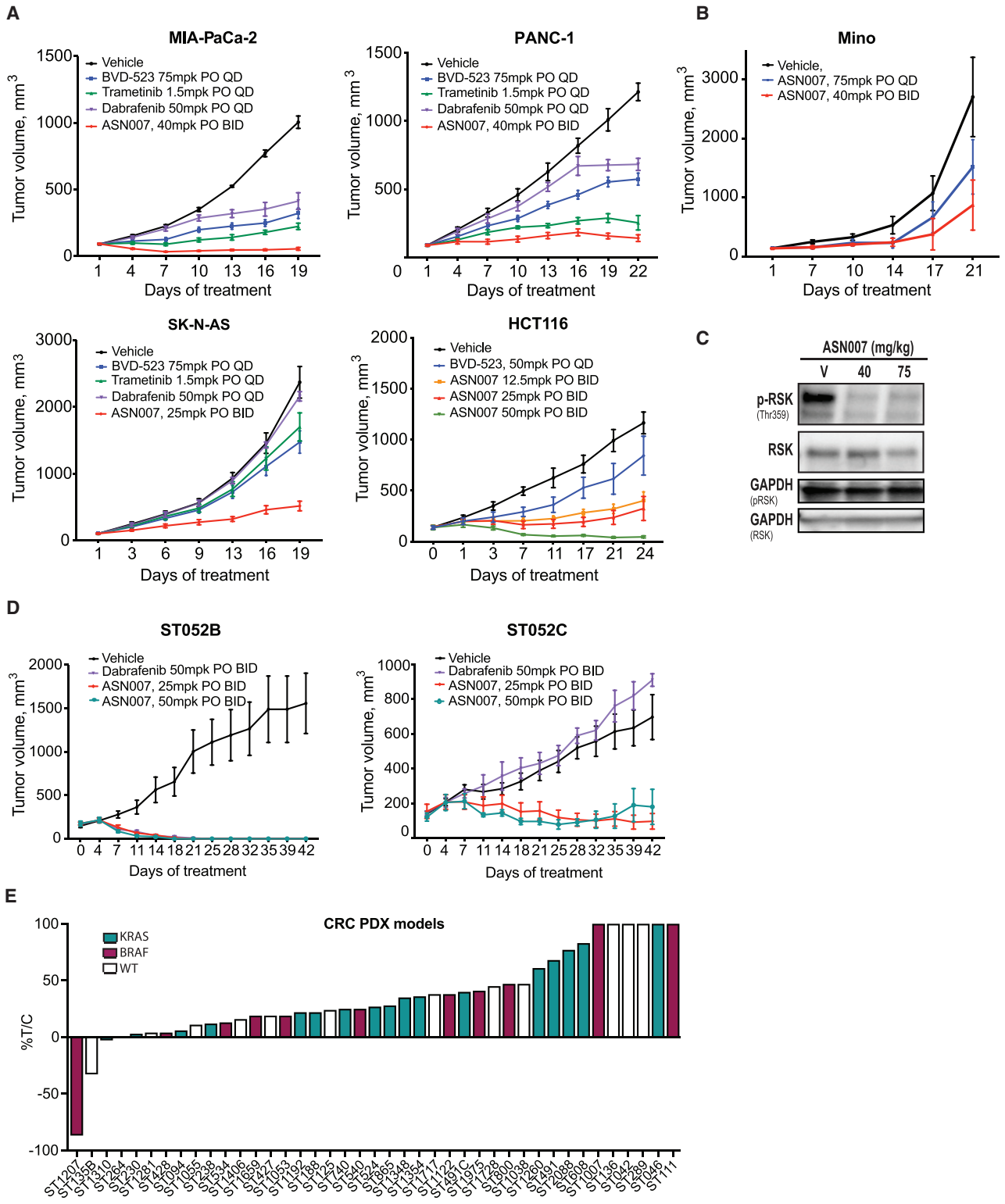

Figure 3. *In vivo* activity of ASN007 in mouse xenografts and PDX models

(A) MIA PaCa-2, PANC-1, SK-N-AS, and HCT116 tumor cells were implanted, and when tumors reached ~100 mm^3 in size, mice were treated with either vehicle or ASN007 at the indicated doses and schedules. BID, twice per day; PO, per os (oral) administration; QD, once per day. Error bars represent means ± SEMs (n > 8 per treatment group).

(legend continued on next page)

mutations: (1) HCT116, a colorectal adenocarcinoma cell line with a $KRAS^{G13D}$ mutation; (2) Panc-1, a pancreatic adenocarcinoma model with a $KRAS^{G12D}$ mutation; (3) MIA PaCa-2, a pancreatic adenocarcinoma model with a $KRAS^{G12C}$ mutation; and (4) SK-N-AS, a neuroblastoma model with a $NRAS^{Q61K}$ mutation. In all four models, ASN007 demonstrated strong antitumor efficacy (Figure 3A) without body weight loss (Figure S2A). Similarly, ASN007 showed a strong tumor growth inhibition in MINO, a mantle cell lymphoma model with a $NRAS^{G13D}$ mutation (Figure 3B). In a pharmacodynamic assay, ASN007 decreased the phosphorylation of ERK1/2 target proteins RSK and MSK (Figure 3C).

The efficacy of ASN007 was evaluated against a panel of 41 patient-derived xenograft (PDX) colorectal cancer mouse models (Figure 3E; Table S3). The panel included 17 tumors with KRAS mutations (including G12C, G12D, G12S, G12V, and G13D), 11 with the $BRAF^{V600E}$ mutation, and 13 with wild-type BRAF and KRAS genes. Overall, treatment with ASN007 resulted in at least 30% tumor growth inhibition in 33 of 41 models (80%) compared to mice treated with vehicle. ASN007 was highly effective in tumors harboring KRAS mutations, as tumor growth inhibition was observed in 16 of 17 models, irrespective of the KRAS subtype mutations. In two $BRAF^{V600E}$ mutant models, ASN007 induced tumor regression below baseline tumor volumes. Using a panel of 45 genes known to be frequently altered in human tumors analyzed by exon sequencing, we observed that most models with mutations in the RAS/MAPK signaling pathway responded to ASN007 treatment (Figure S2B). However, some models with wild-type status of KRAS or BRAF genes also showed sensitivity to ASN007 treatment. Additional studies involving genomics and proteomics would help in understanding the activity of ASN007 in these wild-type models.

In addition, a pair of PDX models were derived from a melanoma patient with a $BRAF^{V600E}$ mutation, one before initiating treatment with vemurafenib and the second established after disease progression while on vemurafenib. In the vemurafenib-sensitive PDX model (ST052B), dabrafenib (50 mg/kg per os [PO] twice per day [BID]) and ASN007 (25 or 50 mg/kg PO BID) demonstrated similar antitumor activity (Figure 3D). In the vemurafenib-resistant PDX model (ST052C), ASN007 (25 or 50 mg/kg PO BID) maintained its antitumor activity with no significant loss of body weight (Figure S2C), whereas dabrafenib showed no efficacy. Thus, ASN007 was effective in both vemurafenib-sensitive and -resistant melanoma PDX models, suggesting that the compound can be used to treat patients with BRAF mutant melanoma after the failure of prior BRAF/MEK inhibitor therapy.

The PI3K inhibitor copanlisib enhances the antitumor activity of ASN007

Interlinked biological network systems such as the RAS/RAF/MEK/ERK and PI3K pathways are reported to be highly responsive to external perturbations, especially when combinational therapies targeting both pathways are used.[19–24] To explore the impact of ERK and PI3K simultaneous inhibition in our models, ASN007-sensitive or ASN007-resistant lymphoma and solid tumor cell lines were treated with different concentrations of ASN007 and the PI3K inhibitor copanlisib.

Combinational therapy enhanced the antiproliferative activity of ASN007 in a variety of lymphoma and solid tumor cell lines compared to either compound alone (Figures 4A, S3A, and S3B). The inhibition of proliferation was associated with the reduced activity of ERK and PI3K downstream targets MSK and ribosomal protein S6 (rS6), respectively. The combination of ASN007 and copanlisib resulted in the suppression of MSK and rS6 phosphorylation to lower levels than are seen with either single-agent treatment (Figure 4B). A similar effect was observed in three different xenograft models (Figure 4C) and in a mantle cell lymphoma (MCL) PDX model (Figure 4D). In all of the models tested, combined therapy led to an enhanced treatment efficacy shown by delayed tumor growth without compromising the body weight of the animals (Figures S3C and S3D).

DISCUSSION

BRAF and MEK inhibitors are the only approved agents targeting RAS/RAF/MEK/ERK signaling activity.[18,25] However, a common feature of these inhibitors is the trigger of compensatory signaling such as the reactivation of ERK1/2, leading to treatment escape and drug resistance.[2,26] These observations suggest that therapeutic targeting of ERK1/2 may have an advantage over inhibiting upstream targets such as MEK or BRAF. In this study, we describe the discovery and characterization of ASN007, an orally bioavailable and potent small-molecule inhibitor of ERK1 and ERK2 kinases.

ASN007 is a reversible and ATP-competitive inhibitor of ERK1/2 kinases. In cell-free assays, ASN007 had an IC_{50} of 2 nM against ERK1 and ERK2 kinases. ASN007 demonstrated antiproliferative activity in an extended panel of solid tumor and lymphoma cell lines, which is associated with the durable blockade

(B) Activity of two different doses of ASN007 in a mantle cell lymphoma xenograft model using the MINO cell line. Error bars represent means ± SEMs (n >8 per treatment group).

(C) Representative western blot analysis of total and phosphorylated ERK1/2 and RSK in tumor extracts from the MINO xenograft at the end of treatment (75 mg/kg, QD, or 40 mg/kg, BID). Glyceraldehyde 3-phosphate dehydrogenase (GAPDH) was used as a loading control.

(D) PDX model derived from a melanoma patient before (ST052B) and after relapsing on vemurafenib treatment (ST052C). In the ST052C model, treatment with ASN007 (25 mg/kg or 50 mg/kg PO, BID) remained effective while therapy with the BRAF inhibitor dabrafenib showed no efficacy. Error bars represent means ± SEMs (n > 5 per treatment group).

(E) Tumor growth inhibition by ASN007 (40 mg/kg PO, BID) in a panel of colorectal cancer PDX models treated for 22 to 35 days, depending on the model. Each bar represents 1 model. The color of the bar denotes the mutation status of BRAF and KRAS genes; magenta = BRAF mutant, green = KRAS mutant, and white = wild type for both BRAF and KRAS. In all *in vivo* efficacy studies except for the HCT116 model, the besylate (salt correction factor 1.33) or mandelate salt form (salt correction factor 1.32) of ASN007 was used. However, the freebase form of ASN007 was used for the study involving the HCT116 model.

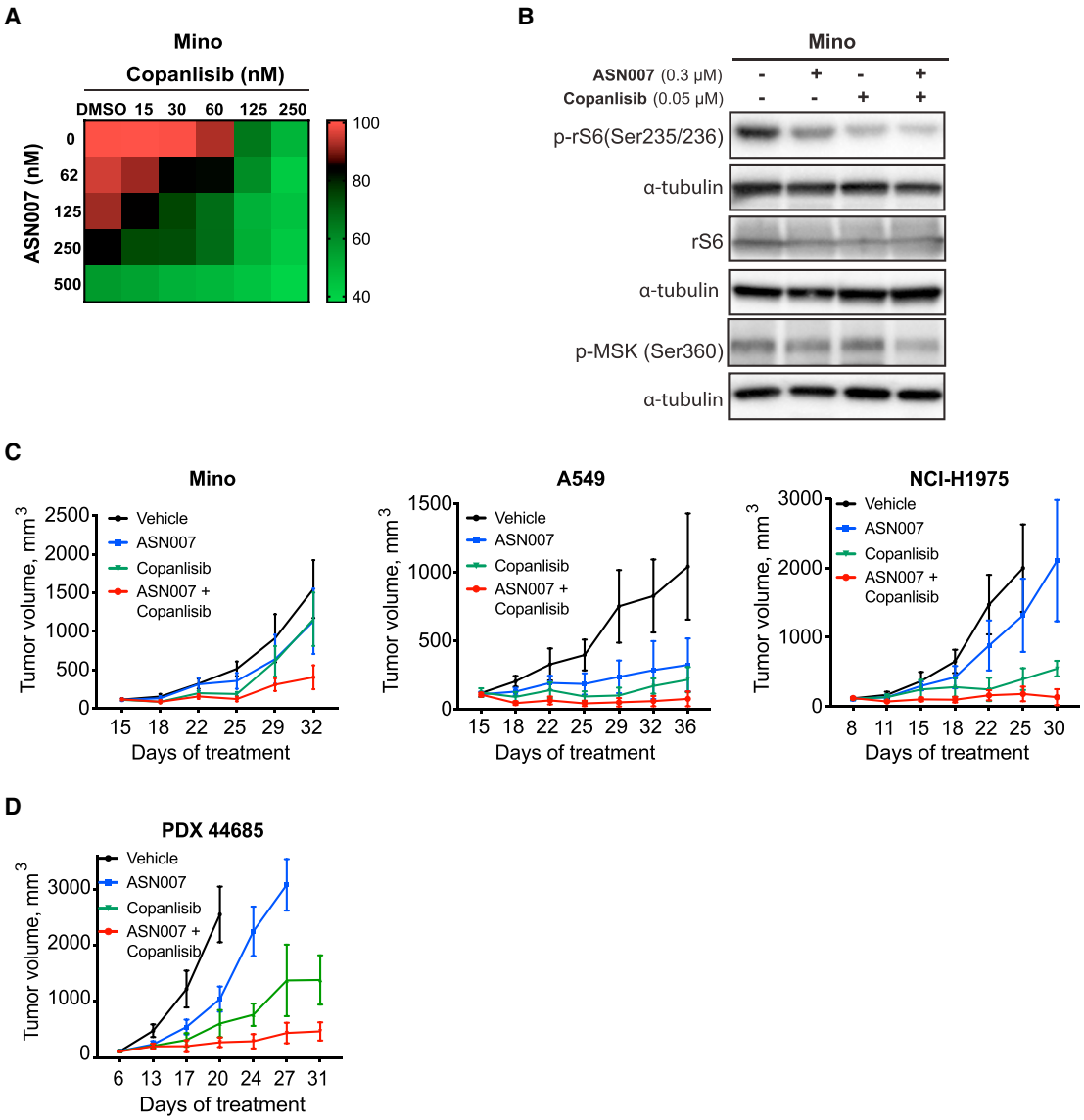

Figure 4. The combination of ASN007 and the PI3K inhibitor copanlisib results in enhanced antiproliferative activity *in vitro* and enhanced tumor growth inhibition *in vivo*

(A) Drug matrix heatmap of the enhanced antiproliferative effect when ASN007 is combined with the PI3K inhibitor copanlisib in an MCL cell line, MINO. Heatmap grids correspond to the mean of three independent experiments measured by the MTS assay.

(B) Western blot analysis of total and phosphorylated levels of rS6 and MSK after 72 h of treatment with ASN007 (0.3 μM), copanlisib (0.05 μM), or the combination of both compounds in MINO cells. Blots are representative of three independent experiments.

(C) Combination of ASN007 and copanlisib results in enhanced efficacy in MINO and two lung carcinoma (A549, NCI-H1975) xenograft tumor models. Error bars represent means ± SEMs (n > 8 per treatment group).

(D) Combination of ASN007 and copanlisib results in enhanced efficacy in an MCL PDX mouse model (PDX44685).

Doses administered: ASN007 (40 mg/kg PO, BID in all four models); copanlisib (14 mg/kg for MINO, NCI-H1975, and PDX 44685, and 10 mg/kg for A549, 2 days on followed by 5 days off, intraperitoneally [i.p.]). Error bars represent means ± SEMs (n > 8 per treatment group).

of ERK target phosphorylation. Furthermore, ASN007 demonstrated preferential activity in a variety of tumor types that harbored mutations in BRAF, KRAS, or RAS, providing a potential selection biomarker in clinical trials. In cell lines harboring mutations in BRAF or RAS, ASN007 demonstrated superior efficacy when compared with other ERK1/2 inhibitors (ulixertinib/BVD-523 and ravoxertinib/GDC-0994).

ASN007 showed potent inhibition of cell proliferation in a panel of cell lines harboring various subtype mutations of KRAS. The subtype mutations include G12C, G12V, G12D, G13D, Q61K, Q61L, Q61H, and Q61R. Several KRAS inhibitors, such as AMG 510, MRTX849, and ARS-3248, are being evaluated in clinical trials (NCT04185883, NCT03785249, and NCT04006301).[27,28] However, these compounds are very specific to the G12C

mutation subtype[27] and do not show activity against other mutant forms of KRAS. Therefore, unlike the $KRAS^{G12C}$ selective inhibitors, ASN007 may have activity in tumors with a broad range of KRAS mutation subtypes.

Despite a remarkable initial response to both BRAF and MEK1/2 inhibitors, most cancer patients subsequently relapse due to acquired resistance.[29,30] Although multiple mechanisms have been identified to mediate this acquired resistance, the ERK1/2 node seems to be the common point of reactivation of the RAS/MAPK pathway.[31,32] This makes ERK1/2 ideal targets for overcoming the resistance to both BRAF and MEK1/2 inhibitors. ASN007 demonstrated strong efficacy in a melanoma PDX tumor model that was resistant to BRAF and MEK1/2 inhibitors. Although the mechanism of resistance to BRAF inhibition in this model is not well characterized, previous studies demonstrate that resistance to BRAF inhibitors is associated with the activation of ERK1/2.[33,34] Therefore, we hypothesized that inhibiting ERK1/2 kinases by ASN007 would be effective in dabrafenib (BRAF inhibitor)-resistant tumor models. Our data suggest that ASN007 could overcome the resistance to BRAF and MEK1/2 inhibitors, and thus, ASN007 may be able to provide a therapeutic option to patients who relapsed on these agents.

Crosstalk between the RAS/MEK/ERK and the PI3K signaling pathways has been reported.[35,36] In addition, MEK inhibition has been shown to cause PI3K activation, and PI3K inhibition has been demonstrated to cause ERK activation.[2,37,38] These observations provided an opportunity to develop a mechanism-based combination strategy combining ASN007 with PI3K inhibitors, such as copanlisib, which was recently approved by regulatory agencies for the treatment of relapsed follicular lymphoma.[39,40] Our data show that the combination of copanlisib and ASN007 was more effective than either drug alone, allowing for the dose reduction of each agent, which may improve treatment tolerance. Moreover, the ASN007 plus copanlisib combination was effective in a variety of tumor models, including breast, lung, and lymphoma cell-line-derived xenografts, in addition to a PDX-model derived from an MCL patient.

In summary, our preclinical data provide a rationale for evaluating ASN007 as a single agent or in combination with PI3K inhibitors in cancer patients, especially those with tumors harboring mutations in RAS and BRAF genes. A phase I study has been conducted in patients with advanced solid tumors harboring BRAF and KRAS, HRAS, and NRAS mutations, and early results suggest that ASN007 is well tolerated with durable clinical activity lasting up to >12 months (NCT03415126).[41]

Limitations of the study

Dose-limiting cytotoxicity remains a challenge with kinase inhibitors. Although we demonstrate that ASN007 performs well by oral delivery either twice or once daily and in combination with a PI3K inhibitor, our study was not designed to address additional organ or systemic toxicities. Further studies should be performed to understand the mechanism of action through which ASN007 is able to overcome resistance to BRAF inhibitors in the melanoma PDX model.

STAR★METHODS

Detailed methods are provided in the online version of this paper and include the following:

- KEY RESOURCES TABLE
- RESOURCE AVAILABILITY
  - Lead contact
  - Materials availability
  - Data and code availability
- EXPERIMENTAL MODEL AND SUBJECT DETAILS
  - Cell lines
  - Human specimens
  - Animals
  - Experimental *in vivo* tumor models
- METHOD DETAILS
  - ERK1/ERK2 homogeneous time-resolved fluorescence (HTRF) enzymatic assay
  - *In vitro* kinase profiling
  - Cell-based target inhibition
  - Cell proliferation assays
  - Western blotting
  - Cell cycle analysis by flow cytometry
- QUANTIFICATION AND STATISTICAL ANALYSIS

SUPPLEMENTAL INFORMATION

Supplemental information can be found online at https://doi.org/10.1016/j.xcrm.2021.100350.

ACKNOWLEDGMENTS

We thank the integrated Genomics Operation Core for the cell lines and PDX samples sequencing and members at the Antitumor Assessment Core for technical assistance. We thank Dhanalakshmi Sivanandhan, Sreekala Nair, Chandru G, Pradeep N, Ramachandraiah Gosu, Krishnakumar V, Sameer Mahmood, Mohd. Zainuddin, and Polina Sai Babu (Jubilant Biosys, Bengaluru, India) for assistance in designing and conducting the experiments. We also wish to thank Michael Wick, Jun Ma, and Morgan Harris from XenoSTART (formerly START) for their help with *in vivo* studies involving melanoma and colorectal cancer PDX models. This work was supported in part by the NIH MSK SPORE in Lymphoma (P50 CA192937), the Leukemia & Lymphoma Society Specialized Center of Research Program (7014-17), Institutional Core Grant (P30 CA008748), and the George Ohrstrom Foundation.

AUTHOR CONTRIBUTIONS

A.P., A.Y., and S.R. designed the experiments and wrote the paper. A.P., M.D.S.F., and Z.A. conducted the experiments. A.K. and V.S. conducted the statistical analysis of the data. E.d.S., S.T., R.A.S., S.G., and L.D. supervised the study and reviewed the manuscript.

DECLARATION OF INTERESTS

A.Y. has received honoraria and/or consultancy fees from Abbvie, Biopath, Curis, Epizyme, Janssen, Merck, Roche, Takeda, and Xynomic and has received research support from Janssen, Curis, Merck, BMS, Syndax, and Roche. S.T., S.G., and L.D. are employees and shareholders of Asana BioSciences. R.A.S. is a shareholder in and consultant to Asana BioSciences. S.T., R.A.S., and S.R. are inventors on three patents covering ASN007 and related compounds and their use in the treatment of cancer. The other authors declare no competing interests.

Received: May 1, 2020
Revised: December 21, 2020
Accepted: June 22, 2021
Published: July 20, 2021

REFERENCES

1. Vogelstein, B., Papadopoulos, N., Velculescu, V.E., Zhou, S., Diaz, L.A., Jr., and Kinzler, K.W. (2013). Cancer genome landscapes. Science *339*, 1546–1558.
2. Samatar, A.A., and Poulikakos, P.I. (2014). Targeting RAS-ERK signalling in cancer: promises and challenges. Nat. Rev. Drug Discov. *13*, 928–942.
3. Montagut, C., and Settleman, J. (2009). Targeting the RAF-MEK-ERK pathway in cancer therapy. Cancer Lett. *283*, 125–134.
4. Wortzel, I., and Seger, R. (2011). The ERK Cascade: Distinct Functions within Various Subcellular Organelles. Genes Cancer *2*, 195–209.
5. Parikh, N., Shuck, R.L., Nguyen, T.A., Herron, A., and Donehower, L.A. (2012). Mouse tissues that undergo neoplastic progression after K-Ras activation are distinguished by nuclear translocation of phospho-Erk1/2 and robust tumor suppressor responses. Mol. Cancer Res. *10*, 845–855.
6. Dhillon, A.S., Hagan, S., Rath, O., and Kolch, W. (2007). MAP kinase signalling pathways in cancer. Oncogene *26*, 3279–3290.
7. McArthur, G.A., Chapman, P.B., Robert, C., Larkin, J., Haanen, J.B., Dummer, R., Ribas, A., Hogg, D., Hamid, O., Ascierto, P.A., et al. (2014). Safety and efficacy of vemurafenib in BRAF(V600E) and BRAF(V600K) mutation-positive melanoma (BRIM-3): extended follow-up of a phase 3, randomised, open-label study. Lancet Oncol. *15*, 323–332.
8. Chapman, P.B., Hauschild, A., Robert, C., Haanen, J.B., Ascierto, P., Larkin, J., Dummer, R., Garbe, C., Testori, A., Maio, M., et al.; BRIM-3 Study Group (2011). Improved survival with vemurafenib in melanoma with BRAF V600E mutation. N. Engl. J. Med. *364*, 2507–2516.
9. Falchook, G.S., Lewis, K.D., Infante, J.R., Gordon, M.S., Vogelzang, N.J., DeMarini, D.J., Sun, P., Moy, C., Szabo, S.A., Roadcap, L.T., et al. (2012). Activity of the oral MEK inhibitor trametinib in patients with advanced melanoma: a phase 1 dose-escalation trial. Lancet Oncol. *13*, 782–789.
10. Delord, J.P., Robert, C., Nyakas, M., McArthur, G.A., Kudchakar, R., Mahipal, A., Yamada, Y., Sullivan, R., Arance, A., Kefford, R.F., et al. (2017). Phase I Dose-Escalation and -Expansion Study of the BRAF Inhibitor Encorafenib (LGX818) in Metastatic *BRAF*-Mutant Melanoma. Clin. Cancer Res. *23*, 5339–5348.
11. Larkin, J., Ascierto, P.A., Dréno, B., Atkinson, V., Liszkay, G., Maio, M., Mandalà, M., Demidov, L., Stroyakovskiy, D., Thomas, L., et al. (2014). Combined vemurafenib and cobimetinib in BRAF-mutated melanoma. N. Engl. J. Med. *371*, 1867–1876.
12. Sanchez, J.N., Wang, T., and Cohen, M.S. (2018). BRAF and MEK Inhibitors: Use and Resistance in BRAF-Mutated Cancers. Drugs *78*, 549–566.
13. Hauschild, A., Grob, J.J., Demidov, L.V., Jouary, T., Gutzmer, R., Millward, M., Rutkowski, P., Blank, C.U., Miller, W.H., Jr., Kaempgen, E., et al. (2012). Dabrafenib in BRAF-mutated metastatic melanoma: a multicentre, open-label, phase 3 randomised controlled trial. Lancet *380*, 358–365.
14. Morris, E.J., Jha, S., Restaino, C.R., Dayananth, P., Zhu, H., Cooper, A., Carr, D., Deng, Y., Jin, W., Black, S., et al. (2013). Discovery of a novel ERK inhibitor with activity in models of acquired resistance to BRAF and MEK inhibitors. Cancer Discov. *3*, 742–750.
15. Blake, J.F., Burkard, M., Chan, J., Chen, H., Chou, K.J., Diaz, D., Dudley, D.A., Gaudino, J.J., Gould, S.E., Grina, J., et al. (2016). Discovery of (S)-1-(1-(4-Chloro-3-fluorophenyl)-2-hydroxyethyl)-4-(2-((1-methyl-1H-pyrazol-5-yl)amino)pyrimidin-4-yl)pyridin-2(1H)-one (GDC-0994), an Extracellular Signal-Regulated Kinase 1/2 (ERK1/2) Inhibitor in Early Clinical Development. J. Med. Chem. *59*, 5650–5660.
16. Kumar, R., Suresh, P.S., Rudresh, G., Zainuddin, M., Dewang, P., Kethiri, R.R., Rajagopal, S., and Mullangi, R. (2016). Determination of ulixertinib in mice plasma by LC-MS/MS and its application to a pharmacokinetic study in mice. J. Pharm. Biomed. Anal. *125*, 140–144.
17. Kidger, A.M., Sipthorp, J., and Cook, S.J. (2018). ERK1/2 inhibitors: new weapons to inhibit the RAS-regulated RAF-MEK1/2-ERK1/2 pathway. Pharmacol. Ther. *187*, 45–60.
18. Liu, F., Yang, X., Geng, M., and Huang, M. (2018). Targeting ERK, an Achilles' Heel of the MAPK pathway, in cancer therapy. Acta Pharm. Sin. B *8*, 552–562.
19. Lehár, J., Krueger, A., Zimmermann, G., and Borisy, A. (2008). High-order combination effects and biological robustness. Mol. Syst. Biol. *4*, 215.
20. Ning, C., Liang, M., Liu, S., Wang, G., Edwards, H., Xia, Y., Polin, L., Dyson, G., Taub, J.W., Mohammad, R.M., et al. (2017). Targeting ERK enhances the cytotoxic effect of the novel PI3K and mTOR dual inhibitor VS-5584 in preclinical models of pancreatic cancer. Oncotarget *8*, 44295–44311.
21. Peng, X., Liu, Y., Zhu, S., Peng, X., Li, H., Jiao, W., Lin, P., Zhang, Z., Qiu, Y., Jin, M., et al. (2019). Co-targeting PI3K/Akt and MAPK/ERK pathways leads to an enhanced antitumor effect on human hypopharyngeal squamous cell carcinoma. J. Cancer Res. Clin. Oncol. *145*, 2921–2936.
22. Won, J.K., Yang, H.W., Shin, S.Y., Lee, J.H., Heo, W.D., and Cho, K.H. (2012). The crossregulation between ERK and PI3K signaling pathways determines the tumoricidal efficacy of MEK inhibitor. J. Mol. Cell Biol. *4*, 153–163.
23. Chappell, W.H., Steelman, L.S., Long, J.M., Kempf, R.C., Abrams, S.L., Franklin, R.A., Bäsecke, J., Stivala, F., Donia, M., Fagone, P., et al. (2011). Ras/Raf/MEK/ERK and PI3K/PTEN/Akt/mTOR inhibitors: rationale and importance to inhibiting these pathways in human health. Oncotarget *2*, 135–164.
24. Wu, Y.L., Maachani, U.B., Schweitzer, M., Singh, R., Wang, M., Chang, R., and Souweidane, M.M. (2017). Dual Inhibition of PI3K/AKT and MEK/ERK Pathways Induces Synergistic Antitumor Effects in Diffuse Intrinsic Pontine Glioma Cells. Transl. Oncol. *10*, 221–228.
25. Yaeger, R., and Corcoran, R.B. (2019). Targeting Alterations in the RAF-MEK Pathway. Cancer Discov. *9*, 329–341.
26. Gibney, G.T., Messina, J.L., Fedorenko, I.V., Sondak, V.K., and Smalley, K.S. (2013). Paradoxical oncogenesis–the long-term effects of BRAF inhibition in melanoma. Nat. Rev. Clin. Oncol. *10*, 390–399.
27. Hallin, J., Engstrom, L.D., Hargis, L., Calinisan, A., Aranda, R., Briere, D.M., Sudhakar, N., Bowcut, V., Baer, B.R., Ballard, J.A., et al. (2020). The KRAS(G12C) Inhibitor MRTX849 Provides Insight toward Therapeutic Susceptibility of KRAS-Mutant Cancers in Mouse Models and Patients. Cancer Discov. *10*, 54–71.
28. Lanman, B.A., Allen, J.R., Allen, J.G., Amegadzie, A.K., Ashton, K.S., Booker, S.K., Chen, J.J., Chen, N., Frohn, M.J., Goodman, G., et al. (2020). Discovery of a Covalent Inhibitor of KRAS(G12C) (AMG 510) for the Treatment of Solid Tumors. J. Med. Chem. *63*, 52–65.
29. Salama, A.K., and Flaherty, K.T. (2013). BRAF in melanoma: current strategies and future directions. Clin. Cancer Res. *19*, 4326–4334.
30. Welsh, S.J., Rizos, H., Scolyer, R.A., and Long, G.V. (2016). Resistance to combination BRAF and MEK inhibition in metastatic melanoma: Where to next? Eur. J. Cancer *62*, 76–85.
31. Van Allen, E.M., Wagle, N., Sucker, A., Treacy, D.J., Johannessen, C.M., Goetz, E.M., Place, C.S., Taylor-Weiner, A., Whittaker, S., Kryukov, G.V., et al. (2014). The genetic landscape of clinical resistance to RAF inhibition in metastatic melanoma. Cancer Discov. *4*, 94–109.
32. Hazar-Rethinam, M., Kleyman, M., Han, G.C., Liu, D., Ahronian, L.G., Shahzade, H.A., Chen, L., Parikh, A.R., Allen, J.N., Clark, J.W., et al. (2018). Convergent Therapeutic Strategies to Overcome the Heterogeneity of Acquired Resistance in $BRAF^{V600E}$ Colorectal Cancer. Cancer Discov. *8*, 417–427.
33. Sullivan, R.J., and Flaherty, K.T. (2013). Resistance to BRAF-targeted therapy in melanoma. Eur. J. Cancer *49*, 1297–1304.
34. Wagle, N., Van Allen, E.M., Treacy, D.J., Frederick, D.T., Cooper, Z.A., Taylor-Weiner, A., Rosenberg, M., Goetz, E.M., Sullivan, R.J., Farlow, D.N., et al. (2014). MAP kinase pathway alterations in BRAF-mutant

melanoma patients with acquired resistance to combined RAF/MEK inhibition. Cancer Discov. *4*, 61–68.

35. Ma, L., Teruya-Feldstein, J., Bonner, P., Bernardi, R., Franz, D.N., Witte, D., Cordon-Cardo, C., and Pandolfi, P.P. (2007). Identification of S664 TSC2 phosphorylation as a marker for extracellular signal-regulated kinase mediated mTOR activation in tuberous sclerosis and human cancer. Cancer Res. *67*, 7106–7112.
36. Yu, C.F., Liu, Z.X., and Cantley, L.G. (2002). ERK negatively regulates the epidermal growth factor-mediated interaction of Gab1 and the phosphatidylinositol 3-kinase. J. Biol. Chem. *277*, 19382–19388.
37. Rozengurt, E., Soares, H.P., and Sinnet-Smith, J. (2014). Suppression of feedback loops mediated by PI3K/mTOR induces multiple overactivation of compensatory pathways: an unintended consequence leading to drug resistance. Mol. Cancer Ther. *13*, 2477–2488.
38. Caunt, C.J., Sale, M.J., Smith, P.D., and Cook, S.J. (2015). MEK1 and MEK2 inhibitors and cancer therapy: the long and winding road. Nat. Rev. Cancer *15*, 577–592.
39. Markham, A. (2017). Copanlisib: First Global Approval. Drugs *77*, 2057–2062.
40. Mensah, F.A., Blaize, J.P., and Bryan, L.J. (2018). Spotlight on copanlisib and its potential in the treatment of relapsed/refractory follicular lymphoma: evidence to date. OncoTargets Ther. *11*, 4817–4827.
41. Tolcher, A.W., Sullivan, R.J., Rasco, D.W., Eroglu, Z., Lakhani, N., Kessler, D., Usansky, H., Reddy, S., Denis, L.J., and Janku, F. (2019). Phase 1 clinical safety and efficacy of ASN007, a novel oral ERK1/2 inhibitor, in patients with RAS, RAF or MEK mutant advanced solid tumors. Mol. Cancer Ther. *18* (*12 Suppl.*), TARG-19-PR09.
42. Wilson, C., Ye, X., Pham, T., Lin, E., Chan, S., McNamara, E., Neve, R.M., Belmont, L., Koeppen, H., Yauch, R.L., et al. (2014). AXL inhibition sensitizes mesenchymal cancer cells to antimitotic drugs. Cancer Res. *74*, 5878–5890.

STAR★METHODS

KEY RESOURCES TABLE

REAGENT or RESOURCE	SOURCE	IDENTIFIER
Antibodies		
Phospho-p90RSK (Thr359)	Cell signaling technology	Cat# 8753; RRID: AB_2783561
RSK1	Cell signaling technology	Cat# 9333; RRID: AB_2181177
p-MSK (S360)	Abcam	Cat# ab81294; RRID: AB_1640701
MSK2	Cell signaling technology	Cat# 3679; RRID: AB_2181641
Phospho-FRA1 (Ser265)	Cell signaling technology	Cat# 3880; RRID: AB_2106922
FRA1 (D80B4)	Cell signaling technology	Cat# 5281; RRID: AB_10557418
α-tubulin	Cell signaling technology	Cat# 3873; RRID: AB_1904178
β-Actin	Sigma	Cat# A5316; RRID: AB_476743
GAPDH (D16H11)	Cell signaling technology	Cat# 5174; RRID: AB_10622025
Phospho-GSK3 β (Ser9)	Cell signaling technology	Cat# 9322; RRID: AB_2115196
Phospho-GSK3 β (Ser21)	Cell signaling technology	Cat# 8452; RRID: AB_10860247
S6 Ribosomal Protein (5G10)	Cell signaling technology	Cat# 2217; RRID: AB_331355
Phospho-S6 Ribosomal Protein (Ser235/236)	Cell signaling technology	Cat# 4856; RRID: AB_2181037
β-catenin	Cell signaling technology	Cat# 9582; RRID: AB_823447
Goat Anti-mouse IgG HRP Conjugate	Biorad	Cat# 170-6516; RRID: AB_11125547
Goat Anti-rabbit IgG HRP Conjugate	Biorad	170-6515; RRID: AB_11125142
Biotinylated rabbit anti-goat IgG	Vector Labs	Cat# BA-5000; RRID: AB_2336126
Biotinylated goat anti-rabbit IgG	Vector Labs	Cat# PK-6101; RRID: AB_2336820
Chemicals, peptides, and recombinant proteins		
ASN007	Asana	N/A
Copanlisib	Selleckchem	Cat# S2802
Dimethyl Sulfoxide	Sigma	Cat# D4540
Palbociclib	Selleckchem	Cat# S1579
Ulixertinib (BVD-523)	Selleckchem	Cat# S7854
SCH772984	Selleckchem	Cat# S7101
Ravoxertinib (GDC-0994)	Selleckchem	Cat# S7554
Trametinib	Selleckchem	Cat# S2673
Dabrafenib	Selleckchem	Cat# S2807
Critical commercial assays		
CellTiter 96 Aqueous Non-Radioactive Cell Proliferation Assay	Promega	Cat# G5430
Supersignal West Dura extended duration substrate	Thermo Fisher	Cat# 34076
3x Blue Loading buffer	Cell signaling technology	Cat# 56036S
30x reducing agent (1.25M DTT)	Cell signaling technology	Cat# 14265S
Matrigel	Thermo Fisher	Cat# CB-40234C
Annexin V FITC Apoptosis detection Kit I	BD Biosciences	Cat# 556547; RRID: AB_2869082
Experimental models: Cell lines		
SU-DHL-6	DSMZ	Cat# ACC-572, RRID:CVCL_2206
JeKo-1	ATCC	Cat# CRL-3006, RRID:CVCL_1865
Mino	ATCC	Cat# CRL-3000, RRID:CVCL_1872
OCI-Ly19	DSMZ	Cat# ACC-528, RRID:CVCL_1878
U-2973	DSMZ	Cat# ACC-642, RRID:CVCL_1898

(*Continued on next page*)

Continued

REAGENT or RESOURCE	SOURCE	IDENTIFIER
SU-DHL-4	DSMZ	Cat# ACC-495, RRID:CVCL_0539
TMD8	Dr. R.E. Davis lab	MDACC
REC-1	ATCC	Cat# CRL-3004, RRID:CVCL_1884
SU-DHL-8	DSMZ	Cat# ACC-573, RRID:CVCL_2207
MAVER-1	DSMZ	Cat# ACC-717, RRID:CVCL_1831
Ri-1	DSMZ	Cat# ACC-585, RRID:CVCL_1885
U-2932	DSMZ	Cat# ACC-633, RRID:CVCL_1896
HBL-1	Dr. R.E. Davis lab	MDACC
Z-138	ATCC	Cat# CRL-3001, RRID:CVCL_B077
NU-DHL-1	DSMZ	Cat# ACC-583, RRID:CVCL_1876
CA46	ATCC	Cat# CRL-1648, RRID:CVCL_1101
EB1	ATCC	Cat# HTB-60, RRID:CVCL_2027
Daudi	ATCC	Cat# CCL-213, RRID:CVCL_0008
L-428	DSMZ	Cat# ACC-197, RRID:CVCL_1361
SUP-M2	Dr. R.E. Davis lab	MDACC
JVM-2	ATCC	Cat# CRL-3002, RRID:CVCL_1319
OCI-Ly3	DSMZ	Cat# ACC-761, RRID:CVCL_8800
BJAB	Dr. R.E. Davis lab	MDACC
KARPAS-299	Dr. R.E. Davis lab	MDACC
Raji	ATCC	Cat# CCL-86, RRID:CVCL_0511
JVM-13	ATCC	Cat# CRL-3003, RRID:CVCL_1318
KM-H2	DSMZ	Cat# ACC-8, RRID:CVCL_1330
DB	DSMZ	Cat# ACC-539, RRID:CVCL_1168
Ramos	ATCC	Cat# CRL-1596, RRID:CVCL_0597
SU-DHL-10	DSMZ	Cat# ACC-576, RRID:CVCL_1889
OCI-Ly10	DSMZ	RRID:CVCL_8795
HT-29	ATCC	Cat# HTB-38, RRID:CVCL_0320
A375	ATCC	Cat# CRL-1619, RRID:CVCL_0132
Colo205	ATCC	Cat# CCL-222, RRID:CVCL_0218
T24	ATCC	Cat# HTB-4, RRID:CVCL_0554
NIC-H2122	ATCC	Cat# CRL-5985, RRID:CVCL_1531
LoVo	ATCC	Cat# CCL-229, RRID:CVCL_0399)
Panc1	ATCC	Cat# CRL-1469, RRID:CVCL_0480
HCT116	ATCC	Cat# CCL-247, RRID:CVCL_0291
Calu6	ATCC	Cat# HTB-56, RRID:CVCL_0236
A549	ATCC	Cat# CRL-7909, RRID:CVCL_0023
NIC-H460	ATCC	Cat# HTB-177, RRID:CVCL_0459
CFPac1	ATCC	Cat# CRL-1918, RRID:CVCL_1119
SK-Mel-2	ATCC	Cat# HTB-68, RRID:CVCL_0069
HepG2	ATCC	Cat# HB-8065, RRID:CVCL_0027
A2780	Millipore Sigma	Cat# 93112519, RRID:CVCL_0134
LnCAP	ATCC	Cat# CRL-1740, RRID:CVCL_1379
PC3	ATCC	Cat# CRL-1435, RRID:CVCL_0035
U87MG	ATCC	Cat# HTB-14, RRID:CVCL_0022
MCF7	ATCC	Cat# HTB-22, RRID:CVCL_0031
T47D	ATCC	Cat# HTB-133, RRID:CVCL_0553
NIC-H1975	ATCC	Cat# CRL-5908, RRID:CVCL_1511

(*Continued on next page*)

Continued

REAGENT or RESOURCE	SOURCE	IDENTIFIER
BT474	ATCC	Cat# HTB-20, RRID:CVCL_0179
786-0	ATCC	Cat# CRL-1932, RRID:CVCL_1051
Experimental models: Organisms/strains		
NSG mice	Jackson Laboratories	N/A
Athymic NU(NCr)-Foxn1 nude	Vivo Biotech	Cat# CRL:490; RRID: IMSR_CRL:490
DLFB-44685	Dana-Farber Cancer institute	Stock # 005557; RRID: IMSR_JAX005557
ST052B	START Center for Cancer Care	N/A
ST052C	START Center for Cancer Care	N/A
Software and algorithms		
Graphpad Prism 8.0	Graphpad software	N/A
CellQuest Pro	BD Biosciences	6.0
FlowJo	BD Biosciences	10
Image lab	Biorad	4.0.1
TREEspot Compound Profile Visualization Tool	DiscoverX	N/A

RESOURCE AVAILABILITY

Lead contact

Further information and requests for resources and reagents should be directed to and will be fulfilled by the Lead Contact, Anas Younes (anas.younes@astrazeneca.com).

Materials availability

All unique/stable reagents generated in this study are available from the Lead Contact with a completed Materials Transfer Agreement.

Data and code availability

The published article includes all datasets generated or analyzed during this study. Kinome screening data generated for this study are summarized on Table S1.

EXPERIMENTAL MODEL AND SUBJECT DETAILS

Cell lines

The human mantle cell lymphoma (MCL) cell lines (REC-1, JeKo-1, Z-138, Mino, JVM-2, JVM-13), Burkitt lymphoma (BL) cell lines (Raji, EB1, DaudiI, Ramos, and CA46) and solid tumors cell lines were obtained from ATCC (American Type Culture Collection). Diffuse large B cell lymphoma (DLBCL)-derived cell lines (SU-DHL-4, SU-DHL-6, SU-DHL-8, SU-DHL-10 OCI-Ly10, DB, NU-DHL-1, U-2973, OCI-Ly3, U-2932, Ri-1 and OCI-Ly19), Hodgkin's cell lines (L-428 and KM-H2) and the MCL cell line MAVER-1 were obtained from the DSMZ-German Collection of Microorganisms and Cell Cultures, Department of Human and Animal Cell Cultures (Braunschweig, Germany). The cell lines BJAB (BL), HBL-1 and TMD8 (DLBCL), SUP-M2, SU-DHL-1 and KARPAS-299 (Anaplastic Large Cell Lymphoma (ALCL)-cell lines) were provided by Dr. R.E. Davis (MD Anderson Cancer Center, Houston, TX). H1975 cells were provided by Dr. M. Ruscetti (Scott Lowe lab, Memorial Sloan Kettering Cancer Center, New York, NY). Lymphoma cell lines were authenticated at the Integrated Genomic Operation Core (Memorial Sloan Kettering Cancer Center, New York, NY). Cell lines were cultured in RPMI 1640 medium supplemented with 10%–20% heat-inactivated fetal bovine serum (Hyclone, GE Healthcare Life Sciences), 1% L-glutamine, and penicillin-streptomycin in a humid environment of 5% CO_2 at 37°C. Mutations were annotated according to CCLE: Cancer Cell Line Encyclopedia (https://www.broadinstitute.org/ccle/home).

Human specimens

Melanoma and colorectal tumor specimens used for PDX were established from primary lesions in patients with cutaneous melanoma and colorectal adenocarcinoma at XenoSTART, San Antonio, US. Mantle cell lymphoma specimen were obtained from Dana-Farber Cancer Institute, Boston, US. Mantle Cell Lymphoma PDX model were utilized for evaluation of ASN007 by the Antitumor Assessment Core at Memorial Sloan Kettering Cancer Center (MSKCC). All PDX were developed and utilized in accordance with Institutional Animal Care and Use Committee approved protocols at XenoSTAR, MSKCC and Dana-Faber and the United States Department of Health and Human Services. Specific informed consent for PDX model generation was obtained from all patients in the

respective institutions of origin (XenoSTART and Dana-Farber). Clinicopathological characteristics PDX model used in this study are summarized in Table S3.

Animals

Experiments were performed in female athymic NU(NCr)-Foxn1 nude mice obtained from Envigo, Charles River Laboratories or Vivo Biotech. The animals were housed in individually ventilated cages (maximum of 4 animals/cage) with 12 hours dark, 12 hours light conditions. The animals were fed food and water *ad libitum*. Temperature and relative humidity were maintained at 20 ± 2°C and 65%, respectively. Female NSG mice were obtained from Jackson laboratory. All animal studies were reviewed and approved by IACUC at Jubilant BioSys, MSKCC and at XenoSTART, Center for Cancer Care. All mice were maintained in accordance with the guidelines of Association for Assessment and Accreditation of Laboratory Animal Care International (AAALAC) on the care, welfare, and treatment of laboratory animals. All experiments met the standards of the Association for the AAALAC, the United States Department of Health and Human Services, and all local and federal animal welfare laws.

Experimental *in vivo* tumor models

Mice randomized 10 mice per treatment groups were injected subcutaneously with specific cell lines, or patient derived (PDX) tumors, which were grown to approximately 100 or 150 mm^3, before they were treated with specified single agents or combinations. Animal body weight and tumor length (L), width (W), and height (H) were measured twice weekly before and during treatment periods on each mouse and then used to calculate tumor volume using the formula (L × W × H)/2. Upon completion of the experiment, tumors were harvested and processed for western blot analysis.

The efficacy of ASN007 in tumor growth inhibition in PDX was evaluated in a panel of colorectal 41 cancer PDX models. The study included wild-type (n = 13), $BRAF^{V600E}$ mutant (n = 10) and KRAS mutant models (n = 18). Out of 18 KRAS mutant models, six of them had PIK3CA mutations. either vehicle group or ASN007 treatment group were treated orally with vehicle or with ASN007 at 25 mg/kg PO, BID for up to 35 days. In all *in vivo* efficacy studies except for the HCT116 model, the besylate (MW = 632.12) or mandelate (MW = 626.09) salt form of ASN007 was used. However, the free base form of ASN007 (MW = 473.94) was used for the HCT116 model.

METHOD DETAILS

ERK1/ERK2 homogeneous time-resolved fluorescence (HTRF) enzymatic assay

Test compounds were serially diluted by half-log dilutions, with concentrations ranging from 0.0005 μM to 10 μM in HTRF assay buffer (50 mM Tris pH = 7.5, 1 mM EGTA, 2 mM DTT, 10 mM $MgCl_2$, 0.1% Tween-20); 20 μL of substrate-ATP mix was added to each well of the assay plate followed by adding 10 μL of enzyme mix to each well. Plates were incubated for 60 min at room temperature with shaking. The HTRF mix was prepared and 75 μL was added to the HTRF plate. After the incubation, 10 μL of the reaction mixture was transferred to the HTRF assay plate and incubated for 45 minutes at room temperature with shaking. Plates were read using the PHERAstar microplate reader in homogeneous time-resolved fluorescence (HTRF) mode. The IC_{50} values were subsequently determined using a sigmoidal dose-response curve (variable slope) in GraphPad Prism 5 software.

In vitro kinase profiling

ASN007 was tested against a panel of 335 protein kinases encompassing both serine/threonine, tyrosine kinases and lipid protein kinases (KinaseProfiler™, Eurofins) in a radiometric assay at a fixed concentration of 1 uM. The residual activity for each kinase was determined using the formula: residual activity (%) = 100 X [(cpm of compound-low control) / (high control – low control)]. The dendrogram was generated using the web tool, TREESpot™, provided by DiscoverX. The 50% inhibitory concentration values (IC_{50}) of ASN007 were determined for the top 22 kinases, which showed > 75% inhibition at 1 μM, selected from the screening panel using 10-point dose response curves at Reaction Biology Corporation.

Cell-based target inhibition

Target inhibition by ASN007 was determined using the solid phase sandwich enzyme-linked immunosorbent assay (ELISA) that detects the levels of RSK1 when phosphorylated at Ser380 position. In this assay, $B\text{-}RAF^{V600E}$ mutant HT29 colon cancer cells were used to test the free base of ASN007 with a potency of 0.007 μM (7 nM). HT29 cells were seeded (60,000 cells/well) in a 96-well plate and incubated at 37°C and 5% CO_2 overnight and then treated with desired compound dilutions for 2 hours. The assay medium was removed, and cells were rinsed once with ice-cold 1X PBS. Then, 0.070 mL ice-cold 1X cell lysis buffer containing 1 mM of the serine protease inhibitor phenylmethanesulfonyl fluoride (PMSF) was added to each well and the plate was incubated on a shaker for 2.5 hours at 4°C. The plate was then centrifuged for 20 minutes (4000 rpm) at 4°C and the supernatant transferred to a new plate. Cell lysates were diluted with sample diluent at a ratio of 1:1. The ELISA was carried out following the manufacturer's protocol. The IC_{50} values were subsequently determined using a sigmoidal dose-response curve (variable slope) in GraphPad Prism 7 software.

Cell proliferation assays

Adherent cells were seeded (5,000 cells/well) in 96-well tissue culture plates and incubated at 37°C and 5% CO_2 for 16 to 24 hours and subsequently treated with different compounds. Compound concentrations ranged from 0.0005 to 10 μM prepared in 3-fold

serial dilutions. The plates were then incubated for 72 hours at 37°C and 5% CO_2. Then Alamar Blue reagent (final concentration 1X) was added to each well and incubated for 1 to 3 hours at 37°C and 5% CO_2. The plates were read on a fluorescence reader at 540 nm excitation and 590 nm emission wavelengths. The IC_{50} values were subsequently determined using a sigmoidal dose-response curve (variable slope) in GraphPad Prism 5 software.

Suspension cells were seeded in 96-well plates at 25,000 cells per 100 μL per well or in 24-well plates at 250,000 cells per 1 mL per well with either vehicle (DMSO 0.1%) or increasing concentrations of compound for 24, 48, and 72 hours. Cell viability was assessed with the nonradioactive cell proliferation MTS assay, using CellTiter 96 AQueous One Solution Reagent (Promega). MTS was added to the culture medium at 1:5 ratios, according to the manufacturer's instructions. Absorbance was recorded at 490 nm with a 96-well plate reader (Bio-Rad) (Molecular Devices, SpectraMax M3). IC_{50} concentrations were calculated from MTS results using GraphPad Prism 7 software.

Western blotting

Preparation of cellular protein lysates or tumor samples was performed by using the Cell Signaling lysis buffer (9803) according to the manufacturer's extraction protocol. Protein quantitation was done using the Direct Detect system (Millipore) or Coomassie Blue reagent following the recommended protocol. A total of 30 μg of protein was denatured in Laemmli buffer supplemented with DTT (10%) at 95°C for 5 min. Western immunoblotting was performed using the Bio-Rad system (TGX 4%–15% gels) or ExpressPlus PAGE 4%–12% gel was assembled in an XCell II Blot module (Invitrogen, Catalog no. EI9051). Transfer was performed for 7 minutes using the Trans Blot turbo system (Bio-Rad) onto PVDF or nitrocellulose membranes. The blots were incubated overnight in 10 mL of blocking buffer (5% BSA in 1X PBS) containing primary antibody. Secondary antibody incubation was done in blocking buffer containing specific IRDye or HRP-conjugate secondary antibody for 1 hour at room temperature and protected from light. Images were acquired by using the Bio-Rad Imaging Chemidoc MP system or Li-Cor Odyssey Imaging system.

Cell cycle analysis by flow cytometry

To determine the effect of ASN007 treatment on cell cycle, cell lines were cultured with or without the ERK1/2 inhibitor for 24 to 72 hours. Cells were collected and then stained with propidium iodide (PI)/RNase staining solution (Cell Signaling, #4087) at room temperature for 15 minutes. Flow cytometric data was acquired on a BD FACSCalibur (BD Biosciences, San Jose, CA) using CellQuest Pro Version 6.0. Propidium iodide was excited by the 488 nm laser and fluorescence emission was measured in fluorescence parameter 3 (FL3) – with the standard 670LP filter. Greater than 10,000 events were acquired. Data Analysis: Doublets were excluded by gating out high FL3- W (width) cells.

QUANTIFICATION AND STATISTICAL ANALYSIS

Procedures to determine the effects of certain conditions on cell proliferation were performed in 3 independent experiments. The two-tailed Student's t test and Wilcoxon rank test were used to estimate the statistical significance of differences between results from the 3 experiments. Significance was set at $p < 0.05$. PRISM software was used for the statistical analyses. For synergy estimation, ΔBliss excess was calculated as shown previously.[42] Bliss expectation was calculated as $A + B - (A \times B)$, where A and B denote the fractional responses from drugs A and B given individually. The difference between Bliss expectation and observed proliferation inhibition of the combination of drugs A and B at the same doses define ΔBliss excess.